Creation of entanglement in a scalable spin quantum computer with long-range dipole-dipole interaction between qubits

D. I. Kamenev,[1] G. P. Berman,[1] and V. I. Tsifrinovich[2]
[1]*Theoretical Division, T-13, and the Center for Nonlinear Studies, Los Alamos National Laboratory, Los Alamos, New Mexico 87545, USA*
[2]*IDS Department, Polytechnic University, Brooklyn, New York 11201, USA*
(Received 20 December 2005; published 29 June 2006)

Creation of entanglement is considered theoretically and numerically in an ensemble of spin chains with dipole-dipole interaction between the spins. The unwanted effect of the long-range dipole interaction is compensated by the optimal choice of the parameters of radio-frequency pulses implementing the protocol. The errors caused by (i) the influence of the environment, (ii) nonselective excitations, (iii) influence of different spin chains on each other, (iv) displacements of qubits from their perfect locations, and (v) fluctuations of the external magnetic field are estimated analytically and calculated numerically. For the perfectly entangled state the z component M of the magnetization of the whole system is equal to zero. The errors lead to a finite value of M. If the number of qubits in the system is large, M can be detected experimentally. Using the fact that M depends differently on the parameters of the system for each kind of error, varying these parameters would allow one to experimentally determine the most significant source of errors and to optimize correspondingly the quantum computer design in order to decrease the errors and $|M|$. Using our approach one can benchmark the quantum computer, decrease the errors, and prepare the quantum computer for implementation of more complex quantum algorithms.

DOI: 10.1103/PhysRevA.73.062336 PACS number(s): 03.67.Lx, 75.10.Jm

I. INTRODUCTION

A quantum computer is supposed to be an analog device designed for implementation of quantum algorithms. The most important algorithm is the Shor's quantum algorithm for factorization of large integer numbers [1,2]. Before experimental realization of this and other complex quantum algorithms, this computer must be tested by implementation of simple algorithms, such as, for example, creation of entanglement with two quantum states (and many qubits). This procedure would allow one to identify the most significant sources of errors and to optimize the quantum computer design.

The following criteria [3] must be met by a physical implementation of a quantum information processor: (i) the qubits must be easy to physically manipulate, (ii) easy to increase the number of qubits, (iii) qubits should interact with each other, (iv) the qubits should be somewhat isolated from environment, and (v) the qubit states must be detectable. Currently, solid state implementations of a quantum computer allow (theoretical) scalability [criterion (ii)] and possibility to substantially increase the number of qubits in the quantum computer register. In a solid state currently one- and two-qubit quantum logic operations are implemented and measured experimentally. Nuclear magnetic resonance and electron spin resonance techniques have been used for quantum information processing in solids. Entanglement between electron and nuclear spins of the same molecule has been implemented and measured in a malonic acid single crystal [4] and in $^{15}N@C_{60}$ endohedral fullerene [5]. Quantum process tomography has been performed on a solid-state qubit represented by a nitrogen-vacancy defect in diamond [6] at room temperature. Initialization (cooling) of nuclear spin has been realized in isotopically labeled malonic acid molecules by a controllable transfer of polarization from neighboring nuclear spins [7,8] at room temperature. One- and two-qubit quantum logic operations have been implemented and measured in superconducting quantum computers [9–11]. A further technological advance can be implementation of simple quantum computing algorithms in a scalable solid state system with a large (more than two) number of qubits for demonstration of basic principles of quantum computation (QC). In this paper, we consider how to implement, probably, the simplest possible algorithm with many qubits: creation of entanglement. To implement this algorithm, we choose one of the most affordable systems: a spin chain placed in a permanent magnetic field with a gradient along the chain. There is a constant dipole-dipole interaction between the qubits. The logic operations are implemented by rectangular radio-frequency pulses. This setup allows one to achieve all criteria (i)–(v).

Indeed, criterion (i) is satisfied because in the system there are no switchable interactions controlled by nanoscopic metal gates, and quantum logic operations are implemented using global addressing technique based on rectangular radio-frequency pulses. Criterion (ii) is satisfied because we consider solid-state QC architectures and because rectangular pulses can be used in the QC with many qubits and all parameters of the applied pulses can be determined analytically. The number of pulses in our entanglement protocol is equal to the number of qubits in the chain. The long-range constant magnetic dipole-dipole interaction satisfies criterion (iii). In the majority of spin-based quantum computer architectures this is the only interaction when neighboring qubits are separated from each other at the distances >1 nm. Criterion (iv) is satisfied because our system allows implementations using qubits with long decoherence times. One possible implementation is based on nuclear spins, for example

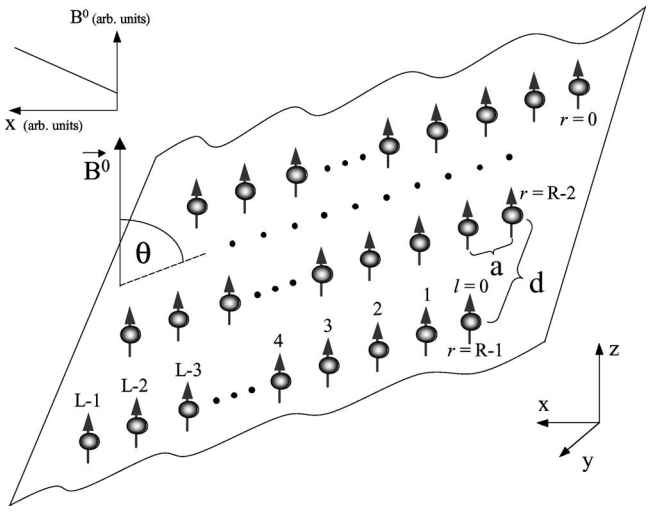

FIG. 1. A setup for creation of entanglement with ensemble of spin chains.

nuclear spins of ^{31}P [12], ^{29}Si [13], or Li [14] in ^{28}Si. Another implementation is based on endohedral fullerenes, $^{15}N@C_{60}$ and $^{31}P@C_{60}$ [15], where the fullerene cage provides a good isolation of electron or nuclear spin of the enclosed atom of nitrogen or phosphorus from the environment. The electrons of the nitrogen or phosphorus atoms have spin 3/2, and the nuclei have spin 1/2 [16,17]. Consequently, our protocols can work only for the nuclear spins of the endohedrals. However, a modification of our scheme for the electrons with spin 3/2 is possible [18]. The third possible implementation is based on electron spins in self-assembled monolayer systems [19–21]. Measurement [criterion (v)] can be performed by using an ensemble of many identical spin chains [19] shown in Fig. 1. The external magnetic field in Fig. 1 is nonuniform in the x direction but uniform in the y direction. Such a gradient can be created by current(s) flowing along the y axis in the plain formed by the chains. Consequently, we take the angle Θ between the qubit plane and the permanent magnetic field to be $\Theta=\pi/2$. If the distance between neighboring chains is sufficiently large all chains experience the same conditions. Consequently, one can create entanglement simultaneously in all chains. If the number of spins in the system is sufficiently large, one can detect the macroscopic magnetization $\vec{\mathcal{M}}$ of the whole system. If each chain is in the entangled state

$$\frac{1}{\sqrt{2}}(|00\cdots00\rangle + e^{i\varphi}|11\cdots11\rangle), \tag{1}$$

then z component $\mathcal{M}_z$ of the macroscopic magnetization must be equal to zero. All possible errors result in deviation of $\mathcal{M}_z$ from its perfect value $\mathcal{M}_z=0$. We will show in this paper that the sign of $\mathcal{M}_z$ and the dependence of $\mathcal{M}_z$ on different parameters of the model can provide us the information about the main source of error. This information can be useful for benchmarking the quantum computer and optimization of its architecture and parameters of quantum protocols.

II. HAMILTONIAN

We consider the implementation of entanglement only for one spin chain of the ensemble of chains illustrated in Fig. 1. Since the chains experience the same conditions the dynamics of all chains is similar. One can neglect the magnetic dipole-dipole interaction between the spins of the different chains when the condition $(a/d)^3 \ll 1$ is satisfied. (Here a is the distance between neighboring qubits of a single chain and d is the distance between different chains, see Fig. 1.) More exact condition of relative independence of different chains will be given in Sec. V C below.

The applied magnetic field has the following components:

$$\vec{B}_n(x,t) = [B^0(x), B_n^1 \cos(\nu_n t + \varphi_n), -B_n^1 \sin(\nu_n t + \varphi_n)],$$

where $B^0(x)$ is a permanent magnetic field and B_n^1, ν_n, and φ_n are, respectively, the amplitude, frequency, and phase of the nth circularly polarized radio-frequency rectangular pulse of a protocol. The permanent magnetic field $B^0(x)$ has a constant gradient $B^0(x_l)=\omega_0+l\delta B^0$, where x_l is the x coordinate of the lth qubit. Note that in practice the magnetic field gradient can be variable. Our results can be easily reformulated for this case, provided that $|B^0(x_l)-B^0(x_{l-1})| \gg B_n^1$. If there is the dipole-dipole interaction between the qubits the Hamiltonian is

$$H_n = H^0 + H_{\rm int} + V_n(t), \tag{2}$$

where

$$H^0 = -\sum_{l=0}^{L-1} \omega_l S_l^z,$$

$$V_n(t) = -\frac{\Omega_n}{2}\sum_{l=0}^{L-1} \{S_l^- \exp[-i(\nu_n t + \varphi_n)] + \text{H.c.}\}, \tag{3}$$

$$H_{\rm int} = -\frac{J}{A^3}\sum_{l=0}^{L-1}\sum_{k=l+1}^{L-1} \frac{1}{(k-l)^3} S_l^z S_k^z,$$

$$J = \frac{\mu^2}{\hbar \mathcal{A}^3}(3\cos^2\Theta - 1) = -\frac{\mu^2}{\hbar\mathcal{A}^3}. \tag{4}$$

Here the Hamiltonian is presented in the frequency units; $\hbar$ is the Planck constant; $S_l^{\pm}=S_l^x \pm iS_l^y$; S_l^x, S_l^y, and S_l^z are the components of the operator of the kth nuclear or electron spin 1/2; $\omega_l=\omega_0+l\delta\omega$, $\omega_0=\gamma B^0(x_0)$, $\delta\omega=\gamma\delta B^0$; $\Omega_n=\gamma B_n^1$ is the Rabi frequency of the nth pulse; $\gamma=\gamma_N$ or $\gamma=-\gamma_e$, where γ_N and γ_e are, respectively, the nuclear and electronic gyromagnetic ratios; $\mathcal{A}=1$ nm, A is the dimensionless parameter equal to the distance between neighboring qubits measured in nanometers, so that $a=A\mathcal{A}$ (a is the distance between neighboring qubits); $\Theta=\pi/2$ is the angle between direction of the spin chain and direction of the permanent magnetic field; $\mu=-g_e\mu_B$ for an electron spin and $\mu=g_N\mu_N$ for a nuclear spin, μ_B and μ_N are, respectively, the Bohr and nuclear magnetons, $g_e \approx 2$ and g_N are, respectively, the electron and nuclear g factors. In Eq. (4) we neglect the x and y components of the dipole-dipole interaction because the

magnetic dipole field on lth qubit in any stationary state $|00\cdots00\rangle$, $|00\cdots01\rangle$,…, is much less than δB^0. So, only the z component of the dipole-dipole field significantly affects the quantum dynamics.

III. CREATION OF ENTANGLEMENT

First, we discuss the formal steps required to create the entangled state. Let the initial state be the ground state $|0_{L-1}0_{L-2}\cdots0_10_0\rangle$ as shown in Fig. 1. We split the ground state into two states by applying the Hadamard transformation

$$\mathcal{H}_0|0_{L-1}0_{L-2}\cdots0_10_0\rangle = \frac{1}{\sqrt{2}}(|0_{L-1}0_{L-2}\cdots0_10_0\rangle + e^{i\phi'}|0_{L-1}0_{L-2}\cdots0_11_0\rangle). \tag{5}$$

Here and below we omit the total phase factor. Then we apply controlled-NOT gate (CNOT_{01}) to the 1st qubit to obtain

$$\frac{1}{\sqrt{2}}(|0_{L-1}0_{L-2}\cdots0_10_0\rangle + e^{i\phi''}|0_{L-1}0_{L-2}\cdots0_21_11_0\rangle). \tag{6}$$

Applying controlled-NOT gates to the remaining $L-2$ qubits we obtain the entangled state

$$\frac{1}{\sqrt{2}}(|0_{L-1}0_{L-2}\cdots0_10_0\rangle + e^{i\phi}|1_{L-1}1_{L-2}\cdots1_11_0\rangle). \tag{7}$$

Below we do not take into consideration the phase factor $e^{i\phi}$. One can make ϕ to be equal to zero by a proper choice of the phases φ_n of the pulses [22].

IV. QUANTUM DYNAMICS

We decompose the wave function into the basis states $|p\rangle$ of the unperturbed Hamiltonian H^0:

$$\psi(t) = \sum_{p=0}^{2^L-1} C_p(t)e^{-iE_pt}|p\rangle, \tag{8}$$

where $|p\rangle=|n_{L-1}n_{L-2}\cdots n_l\cdots n_1n_0\rangle$, $n_l=0,1$, and

$$E_p = \langle p|H^0 + H_{\mathrm{int}}|p\rangle = -\sum_{l=0}^{L-1}\omega_l(p)s_l^z(p) - \frac{J}{A^3}\sum_{l=0}^{L-1}\sum_{k=l+1}^{L-1}\frac{s_l^z(p)s_k^z(p)}{(k-l)^3}. \tag{9}$$

Here $s_l^z(p)$ is the eigenvalue of the operator S_l^z in the state $|p\rangle$: if the lth spin of the state $|p\rangle$ is in the state $|\cdots0_l\cdots\rangle$ then $s_l^z(p)=1/2$ and if the lth spin of the state $|p\rangle$ is in the state $|\cdots1_l\cdots\rangle$ then $s_l^z(p)=-1/2$.

Let the jth spin of the state $|p\rangle$ be in the state $|\cdots0_j\cdots\rangle$ and let the state $|q\rangle$ be associated with the state $|p\rangle$ by flip of the jth spin, $|q\rangle=|\cdots1_j\cdots\rangle$. If the frequency ν_n of the electromagnetic field is close to the Larmor frequency of the jth spin, then under the conditions $|\delta\omega|\gg J/A^3$ and $|\delta\omega|\gg\Omega_n$ the pulse affects mostly this jth spin, and the approximate solution is [23]

$$C_p(t_n+\tau_n) = \left\{\cos\left[\frac{\lambda_n(q,p)\tau_n}{2}\right] + i\frac{\Delta_n(q,p)}{\lambda_n(q,p)}\sin\left[\frac{\lambda_n(q,p)\tau_n}{2}\right]\right\}e^{-i\Delta_n(q,p)\tau_n/2},$$

$$C_q(t_n+\tau_n) = i\frac{\Omega_n}{\lambda_n(q,p)}\sin\left[\frac{\lambda_n(q,p)\tau_n}{2}\right]e^{i\Delta_n(q,p)t_n-i\varphi_n+i\Delta_n(q,p)\tau_n/2},$$

$$C_p(t_n)=1, \quad C_q(t_n)=0, \tag{10}$$

where t_n is the time of the beginning of the nth pulse and

$$\Delta_n(q,p)=E_q-E_p-\nu_n, \quad \lambda_n(q,p)=\sqrt{\Delta_n^2(q,p)+\Omega_n^2}.$$

If the detuning $\Delta_n(q,p)$ is equal to zero, $\Delta_n(q,p)=0$, and for $\Omega_n\tau_n=\pi$ (π pulse), there is a complete transition between the states $|p\rangle$ and $|q\rangle$. Here we neglected the transitions associated with flips of spins with nonresonant transition frequencies for which $l\neq j$. The corrections to the probability amplitude associated with flips of these spins are of order of $\Omega_n/(2|\delta\omega||j-l|)$ [24,25]. These corrections are small provided $\Omega_n/|\delta\omega|\ll1$.

Controlled--NOT gate for the system with long-range dipole-dipole interaction. Since the entanglement is implemented by a sequence of controlled-NOT (CNOT) gates we now derive the parameters required to implement these gates taking into consideration the long-range interaction. Because of this interaction the action of the controlled-NOT gate on the jth qubit depends not only on the states of $(j-1)$th and $(j+1)$th qubits, but also on the states of distant lth qubits, where $l\neq j-1,j,j+1$. Consequently, it is convenient to formulate the controlled-NOT gate CNOT not in terms of the states of the corresponding qubits, like $\mathrm{CNOT}_{j-1,j}$, but in terms of the eigenstates $|p\rangle$ of the Hamiltonian H^0. For example, the gate $\mathrm{CNOT}_j(p,q)$ flips the jth qubit for the state $|p\rangle$ and completely suppresses flip of the same jth qubit for the state $|q\rangle$. This procedure allows one to compensate the unwanted action of the long-range interaction by an optimal choice of the parameters of the pulses. Our approach works for the case when there are only two "working states" (excluding error unwanted states) in the quantum register. It is useful for creation of entanglement with two states introduced in Sec. III. If there are more than two states in the quantum register, more complex (shaped) pulses are required to minimize the effect of the long-range interaction.

Let us write the entangled state in the form $(1/\sqrt{2})(|0\rangle+|p'\rangle)$, where $|0\rangle$ is the ground state and $|p'\rangle$ is the excited state. The pulses of the protocol must suppress the transitions from the ground state and to implement the transitions for the excited states, so that the state $|p'\rangle$ evolves as

$$|p'\rangle: |000\cdots001\rangle\rightarrow|000\cdots011\rangle\rightarrow|000\cdots0111\rangle\rightarrow\cdots\rightarrow|001\cdots111\rangle\rightarrow|011\cdots11\rangle\rightarrow|111\cdots11\rangle. \tag{11}$$

The controlled-NOT gates implementing these transitions are $\mathrm{CNOT}_j(p',0)$, where $j=1,2,\ldots,L-1$ is the number of the spin to be flipped in the excited state $|p'\rangle$ and also the num-

ber of the corresponding π pulse. (We do not count the initial $\pi/2$ pulse.)

We now derive the parameters of the initial pulse implementing the Hadamard transform. In order to flip the 0th spin in the ground state the detuning must be equal to zero, $E_1 - E_0 - \nu_H = 0$, where ν_H is the frequency of the pulse. Using Eq. (9) we obtain

$$\nu_H = E_1 - E_0 = \omega_0 + \frac{J}{2A^3}\sum_{l=1}^{L-1}\frac{1}{l^3}. \tag{12}$$

The Rabi frequency Ω_H of the initial pulse must satisfy the condition $\Omega_H \ll \delta\omega$ and the time duration of the pulse is $\tau_H = \pi/(2\Omega_H)$.

Consider now the controlled-NOT gate $\mathrm{CNOT}_j(p',0)$. If the state $|q'\rangle$ is associated with the state $|p'\rangle$ by a flip of the jth spin, the frequency is

$$\nu_j = E_{q'} - E_{p'} = \omega_j + \frac{J}{A^3}\sum_{\substack{l=0\\ l\neq j}}^{L-1}\frac{s_l^z(p')}{|l-j|^3}. \tag{13}$$

For example, for $j=1$, one has $s_0^z(p') = -1/2$ and $s_l^z(p') = 1/2$ for $l = 2,3,\ldots,L-1$, so that the frequency of the first π pulse is

$$\nu_1 = \omega_1 + \frac{J}{2A^3}\sum_{l=3}^{L-1}\frac{1}{(l-1)^3},$$

the frequency of the second π pulse is

$$\nu_2 = \omega_2 + \frac{J}{2A^3}\sum_{l=5}^{L-1}\frac{1}{(l-2)^3},$$

and so on.

In order to suppress the unwanted transitions from the ground states one can use a $2\pi K$ method [2,26,27]. Here we will modify this method so that it can be applied to the system with the long-range interaction. As follows from Eq. (10) the transition with nonzero detuning is suppressed if the value of the sine is equal to zero, i.e., when

$$\Omega_j = \frac{|\Delta_j(q'',0)|}{\sqrt{4K^2-1}}, \tag{14}$$

where $K = 1,2,\ldots$ and the state $|q''\rangle$ is associated with the ground state by a flip of the jth spin. Using Eq. (9) we find

$$E_{q''} - E_0 = \omega_j + \frac{J}{A^3}\sum_{\substack{l=0\\ l\neq j}}^{L-1}\frac{s_l^z(0)}{|l-j|^3} = \omega_j + \frac{J}{2A^3}\sum_{\substack{l=0\\ l\neq j}}^{L-1}\frac{1}{|l-j|^3}.$$

From Eq. (13) we obtain the detuning

$$\Delta_j(q'',0) = E_{q''} - E_0 - \nu_j = \frac{J}{A^3}\sum_{\substack{l=0\\ l\neq j}}^{L-1}\frac{s_l^z(0) - s_l^z(p')}{|l-j|^3} = \frac{J}{A^3}\sum_{l=0}^{j-1}\frac{1}{(j-l)^3}. \tag{15}$$

We note that if the long-range dipole-dipole interaction is not taken into consideration, then the error to the probability amplitude generated by each pulse due to the next-nearest-neighbor interaction is of the order of $(1/2)^3 = 1/8$. Our approach allows us to compensate the unwanted effect of the long-range interaction by optimal choice of the parameters of the pulses.

V. ERRORS AND z COMPONENT OF THE MAGNETIZATION

The protocol consisting of rectangular pulses with the parameters defined by Eqs. (12)–(15) allows one to implement entanglement in the ensemble of noninteracting spin chains with minimum possible error P. It is possible to relate the error P with the z component $\mathcal{M}_z$ of the magnetization of the system. Since $\mathcal{M}_z$ is caused by the error states, then one can assume that $\mathcal{M}_z \sim P$. We define the dimensionless z component of the magnetization $M \sim \mathcal{M}_z$ in the following way. Let the maximum value of $|M|$ be 1. Then for the state $|00\cdots00\rangle$ we have $M=1$ and for the state $|11\cdots11\rangle$ we have $M=-1$. The measured z component of the magnetization of the system shown in Fig. 1 corresponding to M is $\mathcal{M}_z = \frac{1}{2}M\mu RL$.

In this section we will estimate and compare contribution of different kinds of errors to the total error P and relate these errors with M. Since we can estimate P analytically for a large number of qubits, the relation between M and P allows us to estimate M for $L \gg 1$. Different kinds of errors can generate positive and negative contributions to M so that they can cancel each other. For example, the state $C_p(|000111\rangle + |111000\rangle)$ contributes to P but does not contribute to M. In spite of this we assume that for a definite range of parameters the relation $M = gP$ holds [see Eq. (24) below], where the coefficient g is the "geometrical factor" and P is the probability of error. For example, if a single spin in the state $(1/\sqrt{2})|0000\rangle$ of superposition (1) is flipped down with the probability P then $g = -1/L = -1/4$. If two spins are flipped down with the probability P then $g = -2/L = -1/2$. If a single spin in the state $(1/\sqrt{2})|1111\rangle$ is flipped up then $g = 1/L = 1/4$ and so on. If, for example, different spins in the state $(1/\sqrt{2})|0000\rangle$ have different probabilities P_j to be flipped then $M = (-1/L)\Sigma_{j=0}^{3}P_j$ [see Eqs. (46) and (51) below].

The probability of error P depends on parameters and number of qubits L. This dependence is different for different kinds of errors. For example, for nonresonant transitions $P \sim L$ [see Eq. (20) below]. By experimental measurement of M for different parameters one can define the most important mechanism responsible for the errors. Using this information one can optimize the design and parameters to decrease the error and to prepare a quantum computer for implementation of complex quantum algorithms.

A. Decoherence

The influence of environment can be characterized by the temperature-dependent spin-lattice relaxation time T_1 and spin-spin relaxation time T_2, where $T_2 \leqslant T_1$. The relaxation time T_2 defines the maximum number of pulses and consequently the maximum number $L_{\max}$ of qubits in each spin chain. Increasing $L_{\max}$ is desirable for increasing the number of qubits in the quantum register and for better measurement (because the total magnetization of the ensemble of the spin chains is proportional to $L_{\max}$). We note that the number of the spin chains $R_{\max}$ theoretically is not limited, so that the size of the whole system and the total number of spins can be increased by increasing R. If $L \ll L_{\max}$ the influence of environment is small and one can formulate quantum dynamics in terms of wave function instead of using density matrix. This allows one to consider quantum logic operations with many qubits [23,25,28] and to analytically estimate the influence of other sources of error which, as shown below, can cause a much more profound destructive effect on quantum computation.

We define $L_{\max}$ from the condition

$$\tau_H + \sum_{j=1}^{L_{\max}-1} \tau_j \leqslant T_2, \tag{16}$$

where $\tau_j = \pi/\Omega_j$. The pulse performing the Hadamard transform can be made very short by increasing the amplitude B_H^1 of this pulse, so that we will neglect contribution of τ_H. Using Eqs. (14)–(16) we obtain

$$\sum_{j=1}^{L_{\max}-1} \left(\sum_{l=0}^{j-1} \frac{1}{(j-l)^3} \right)^{-1} \leqslant \frac{|J|T_2}{\pi A^3 \sqrt{4K^2-1}}. \tag{17}$$

The left-hand side for $L_{\max} \gg 1$ can be approximated as

$$\sum_{j=1}^{L_{\max}-1} \left(\sum_{l=0}^{j-1} \frac{1}{(j-l)^3} \right)^{-1} \approx \frac{L_{\max}-1}{\zeta(3)} + 0.3399, \tag{18}$$

where $\zeta(3) \approx 1.202057$, and $\zeta(x)$ is the Riemann zeta function.

We now estimate $L_{\max}$ for endohedral fullerenes. The very sharp electron spin resonance spectra from the endohedrals $^{15}N@C_{60}$ and $^{31}P@C_{60}$ indicates very long longitudinal relaxation time $T_1 \sim 10$ ms at the temperature $\mathcal{T}=10$ K, and $T_1 \sim 0.9$ ms at $\mathcal{T}=300$ K. The transverse relaxation time is $T_2 \sim 20$ μs at $\mathcal{T}=50$ K and $T_2 \sim 13$ μs at $\mathcal{T}=300$ K [29]. No nuclear relaxation times have yet been recorded but they are expected to be several orders of magnitude longer than the electronic relaxation times. We will make our estimation of $L_{\max}$ for the electron spins. The value of the coupling constant $|J_e|$ for two electron spins is $(\mu_B = 9.274 \times 10^{-21}$ erg/G$)|J_e|/(2\pi) \approx 52$ MHz. The minimum distance between two endohedrals is close to the diameter of the C_{60} cage (1 nm) and can be as small as 1.1 nm [18]. Taking $K=1$, $T_2=20$ μs, and $A=2.2$, the right-hand side of Eq. (17) becomes equal to 113. From Eq. (18) this value corresponds to $L_{\max}=136$. The value of $L_{\max}$ decreases when the distance A between neighboring endohedrals increases.

Due to the interaction of the spin system with the environment M becomes positive. The reason is that the energy of the state $|1\rangle$ is larger than the energy of the state $|0\rangle$, so that the influence of the environment causes the transitions $|1\rangle \rightarrow |0\rangle$ while the transitions $|0\rangle \rightarrow |1\rangle$ are suppressed.

B. Nonresonant transitions

Since wavelength of the radio-frequency pulses is much larger than the size of the quantum register, the pulses affect all spins. If the pulse frequency is close to the frequency ω_j of jth spin then the probability of flipping kth spin, $k \neq j$ is of order of [24]

$$\epsilon_{jk} = \left(\frac{\Omega_j}{2|j-k|\delta\omega} \right)^2.$$

The probabilities of the nonresonant transitions are small provided that the ratio $\Omega_j/(2|\delta\omega|)$ is small. Using Eqs. (14) and (15) we obtain

$$\epsilon_{jk} \sim \frac{\alpha^2}{4(j-k)^2}, \quad \alpha = \frac{|J|}{\sqrt{4K^2-1}A^3|\delta\omega|}. \tag{19}$$

The probabilities of unwanted quantum states created in the result of the nonresonant transitions are of the order of α^2, and the probability error $P_{\rm nr}$ caused by the nonselective excitations is proportional to α^2. The error $P_{\rm nr}$ grows linearly with the number of pulses L [28]. A typical behavior of $P_{\rm nr}(L)$ is shown in Fig. 2 for a small number of qubits L and for two values of α: $\alpha=0.02$ and $\alpha=0.09$. For example, for two electron spins with $|J|/(2\pi)=52$ MHz separated by the distance 2.2 nm and for $K=1$ these values of α correspond, respectively, to $|\delta\omega|/(2\pi)=141$ MHz and $|\delta\omega|/(2\pi)=31.4$ MHz. These values of $\delta\omega$ correspond, respectively, to the following magnetic field gradients $[\delta\omega=\gamma_e \delta B^0, \gamma_e/(2\pi) \approx 28.025$ GHz/T]: 2.3×10^6 and 5.1×10^5 T/m, which can be realized experimentally [30–33].

Comparison of Fig. 2(a) with Fig. 2(b) indicates the importance of the strong magnetic field gradient in keeping the error small in the system with a large number of qubits. As follows from the figures, increasing L, for example, to $L=100$ results in the error of the order of 70% for $\alpha=0.09$ and the error of the order of 4% for $\alpha=0.02$.

We approximate $P_{\rm nr}$ as

$$P_{\rm nr}(L) = -P_{\rm nr}^0 + P_{\rm nr}^1 L, \quad L > 2. \tag{20}$$

The values of $P_{\rm nr}^0$ and $P_{\rm nr}^1$ found numerically are shown in Fig. 3. The numerical simulations are performed by diagonalization of the full Hamiltonian H_n given by Eq. (2) for each nth pulse in the rotating frame where H_n is time independent. The obtained eigenstates were used for simulation of the quantum dynamics [26]. The best fit obtained from the data presented in Fig. 3 gives us the expressions

$$P_{\rm nr}^0 = 0.8236\alpha^{1.988}, \quad P_{\rm nr}^1 = 0.8615\alpha^{1.987}, \quad \alpha \ll 1. \tag{21}$$

In Fig. 2 we use these parameters to approximate the function $P_{\rm nr}(L)$. One can see that there is a good correspondence between the numerical results and our estimate (20). Our

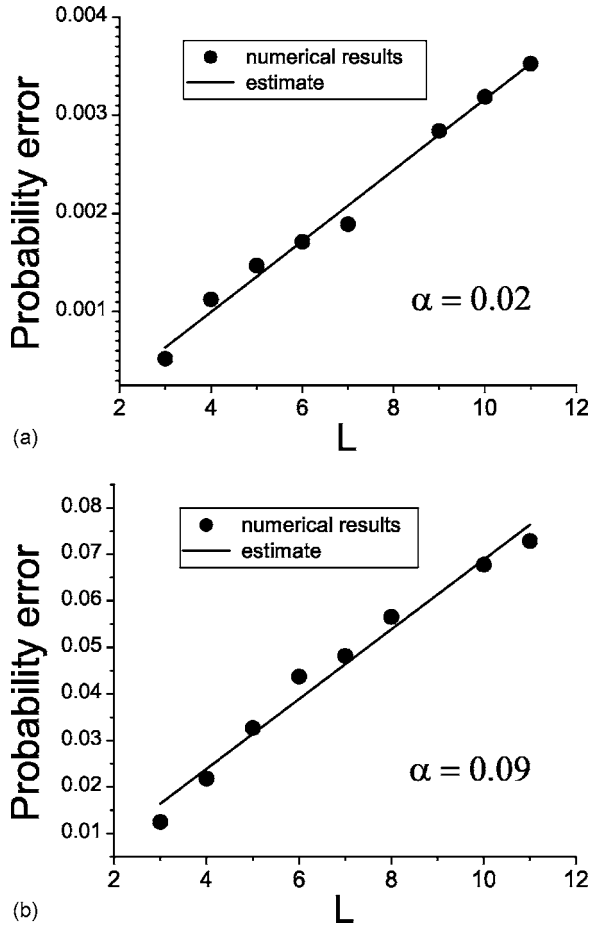

FIG. 2. The probability error $P_{\rm nr}$ obtained using numerical solution [25] and estimate using Eqs. (20) and (21) as a function of the number of qubits L for two values of α.

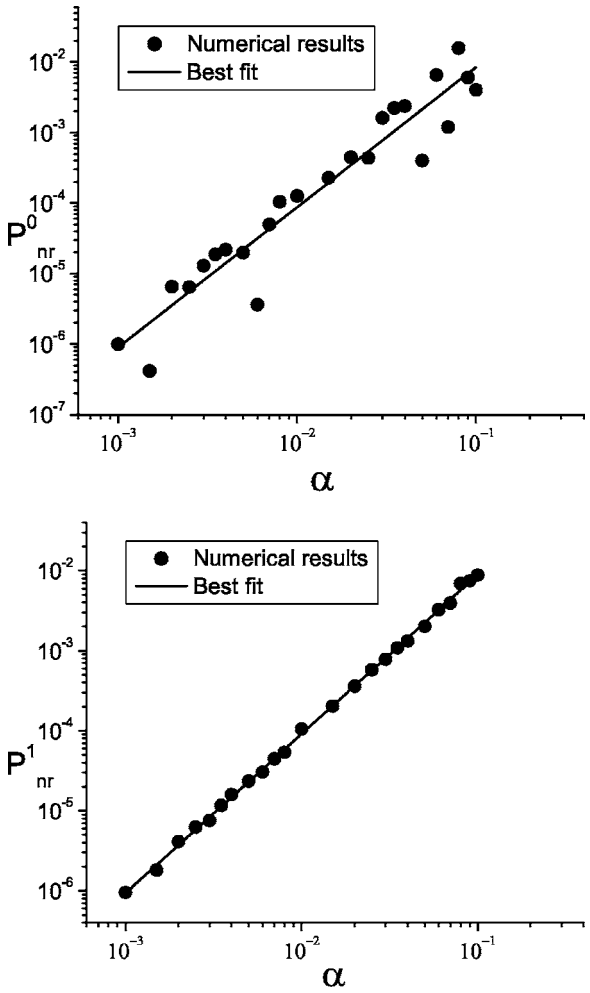

FIG. 3. $P^0_{\rm nr}$ and $P^1_{\rm nr}$ in Eq. (20) obtained using numerical solution and the best fits with the parameters defined by Eq. (21).

estimate (20) is especially useful when L is large, $L\sim 10^2-10^3$, when no exact solution is available.

Since the z component of the magnetization $M_{\rm nr}$ is proportional to $P_{\rm nr}$ it is reasonable to present the dependence of $M_{\rm nr}$ on L in the form

$$M_{\rm nr}=M^0_{\rm nr}-M^1_{\rm nr}L. \tag{22}$$

A typical behavior of $M_{\rm nr}$ as a function of L is shown in Fig. 4 for two values of α. From this figure one can see that $M_{\rm nr}$ is negative.

From Fig. 4 one can numerically calculate $M^0_{\rm nr}$ and $M^1_{\rm nr}$. We calculated M_0 and M_1 for different values of α (see Fig. 5) and obtained

$$M^0_{\rm nr}=1.341\alpha^{2.044},\quad M^1_{\rm nr}=0.60786\alpha^{1.9795},\quad \alpha\ll 1. \tag{23}$$

From Fig. 3 one can see that Eq. (22) with parameters (23) gives us a good approximation of $M_{\rm nr}$. It is important that the number of qubits in Eqs. (20) and (22) is an explicit parameter, so that one can calculate the probability errors and z component of the magnetization due to the nonresonant transitions for an arbitrary number of qubits L. Combining Eqs. (20) and (22) we obtain the relation between $M_{\rm nr}$ and $P_{\rm nr}$

$$M_{\rm nr}=g^0_{\rm nr}+g^1_{\rm nr}P_{\rm nr}, \tag{24}$$

where

$$g^0_{\rm nr}=M^0_{\rm nr}-\frac{P^0_{\rm nr}}{P^1_{\rm nr}}M^1_{\rm nr},\quad g^1_{\rm nr}=-\frac{M^1_{\rm nr}}{P^1_{\rm nr}}.$$

C. Interaction between different chains

Here we will discuss the possibility to decrease the influence of the chains on each other by optimal choice of the parameters of the pulses. We will show that if the long-range interaction between the chains is not taken into consideration the influence of the chains on each other causes the error of the order of $L(a/d)^3$. Consider the jth spin of the rth spin chain in the field of the spins of the $(r-1)$th, rth and $(r+1)$th chains. (See Fig. 6.) The resonant frequency is [compare with Eq. (13)]

$$\nu_j=\omega_j+\frac{J}{A^3}\sum_{\substack{l=0\\ l\neq j}}^{L-1}\frac{s^z_l(p')}{|l-j|^3}+\frac{2J}{D^3}\sum_{\substack{l=0\\ l\neq j}}^{L-1}\frac{s^z_l(p')}{[1+\chi^2(j-l)^2]^{3/2}}, \tag{25}$$

where D is the dimensionless distance between neighboring chains measured in nanometers and $\chi=a/d=A/D\ll 1$. The

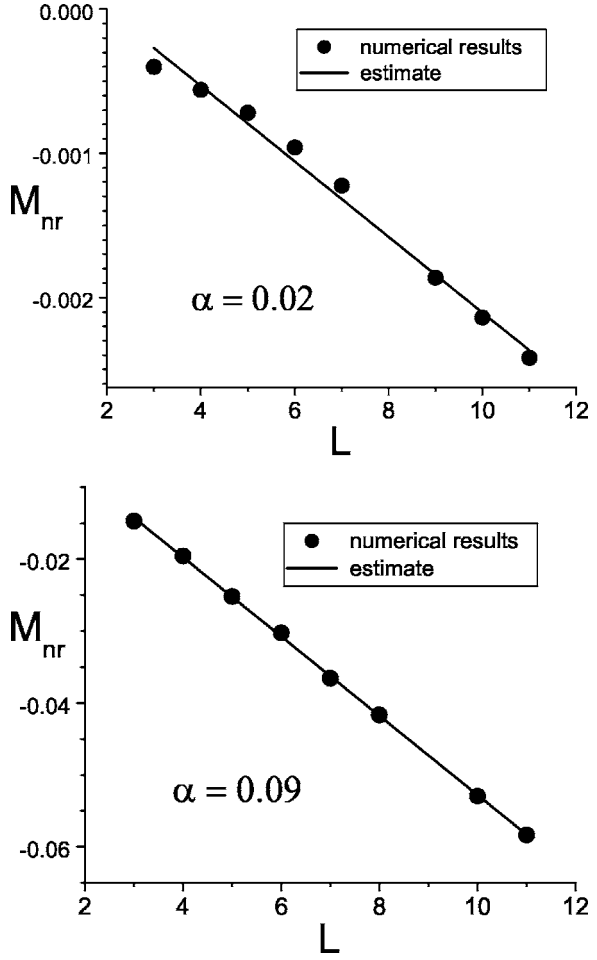

FIG. 4. The dimensionless z component M_{nr} of the magnetization generated in result of the nonresonant transitions as a function of the number of qubits L for two values of α. The estimates are calculated using Eq. (22) with the parameters defined by Eq. (23).

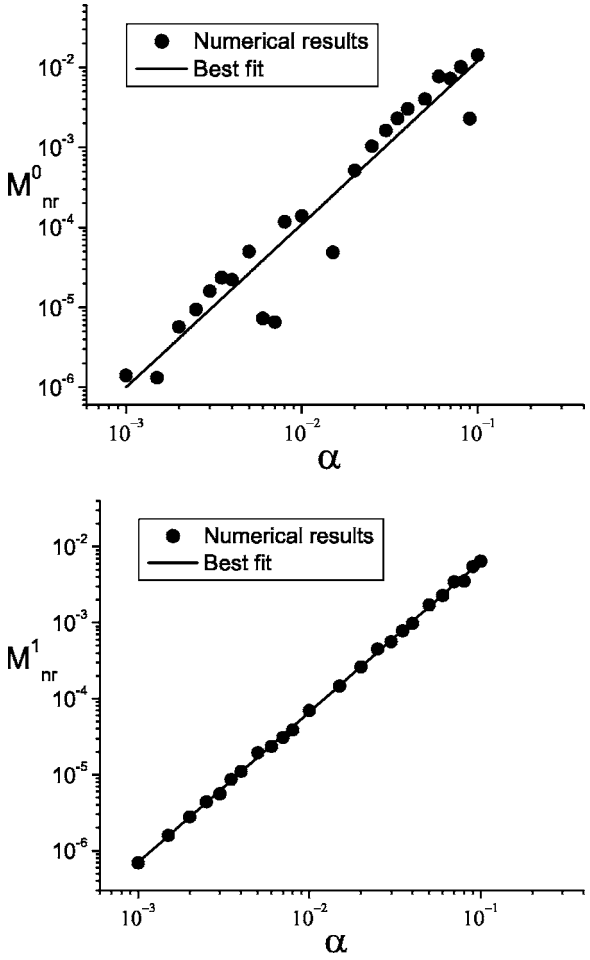

FIG. 5. M^0_{nr} and M^1_{nr} as a function of α. The best fit gives the parameters defined by Eq. (23).

Rabi frequency of the pulse is [see Eqs. (14) and (15)]

$$\Omega_j = \frac{|J|}{A^3\sqrt{4K^2-1}}\sum_{l=0}^{j-1}\frac{1}{(j-l)^3} + \frac{2|J|}{D^3\sqrt{4K^2-1}}\sum_{l=0}^{j-1}\frac{1}{[1+\chi^2(j-l)^2]^{3/2}}. \quad (26)$$

We now can estimate the error caused by the influence of different chains on each other if we neglect the interaction between them. Consider the resonant transition for the excited state of the superposition using Eq. (10). If we disregard the influence of the neighboring chains on each other, then instead of the resonant transition with $\Delta_j(q',p')=0$ we have the nonzero contribution of the third term in Eq. (25)

$$|\Delta_j(q',p')| = \frac{2|J|}{D^3}\left|\sum_{\substack{l=0\\ l\neq j}}^{L-1}\frac{s_l^z(p')}{[1+\chi^2(j-l)^2]^{3/2}}\right|.$$

Since the value of the sine in the first Eq. (10) is of the order of unity and the value of the cosine is close to zero, the value

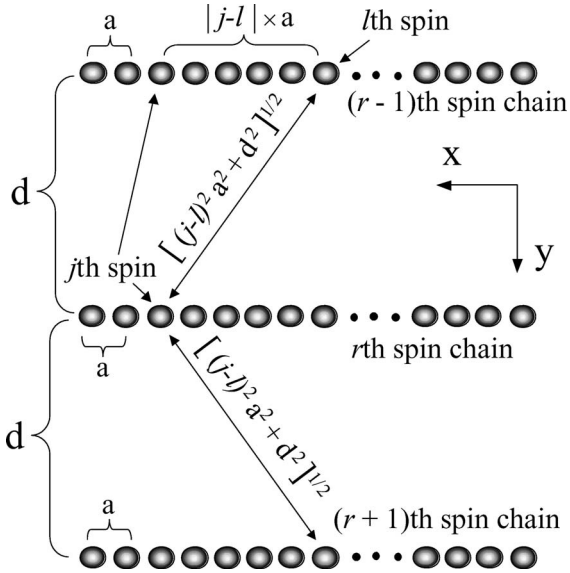

FIG. 6. A scheme for calculation of the influence of the lth spin of the $(k-1)$th and $(k+1)$th spin chains on the jth spin of the kth spin chain.

of the coefficient $C_P(t_j+\tau_j)$ is of the order of (instead of zero in the ideal case)

$$|C_{p'}(t_j+\tau_j)| \approx \left|\frac{\Delta_j(q',p')}{\lambda_j(q',p')}\right| \approx \left|\frac{\Delta_j(q',p')}{\Omega_j}\right| \approx 2\sqrt{4K^2-1}\chi^3 \left|\sum_{\substack{l=0 \\ l\neq j}}^{L-1} \frac{s_l^z(p')}{[1+\chi^2(j-l)^2]^{3/2}}\right| \times \left[\sum_{l=0}^{j-1}\frac{1}{(j-l)^3}\right]^{-1}. \quad (27)$$

The error P_{int} caused by the influence of neighboring chains on each other is of the order of $P_{\text{int}}=|C_{p'}(t_j+\tau_j)|^2$. From Eq. (27) one can see that P_{int} increases with the Rabi frequency Ω_j decreasing.

In order to estimate the error in the probability amplitude given by Eq. (27) consider a typical example. Let the distance between the chains be equal to the size of a single chain, $d=(L-1)a$ $[D=(L-1)A]$, $L\gg 1$. Then $\chi=1/(L-1)$. Let us estimate $\sqrt{P_{\text{int}}}$ for $j=L-1$. The first sum in Eq. (27) is

$$-\frac{1}{2}\sum_{l=0}^{L-2}\frac{1}{[1+\chi^2(L-1-l)^2]^{3/2}} = -\frac{1}{2}\sum_{l=0}^{L-2}\left[1+\left(1-\frac{l}{L-1}\right)^2\right]^{-3/2}.$$

For all terms of the sum we have

$$\frac{1}{2^{3/2}} \leqslant \left[1+\left(1-\frac{l}{L-1}\right)^2\right]^{-3/2} < 1,$$

so that

$$\frac{L-1}{2^{3/2}} < \sum_{l=0}^{L-2}\left[1+\left(1-\frac{l}{L-1}\right)^2\right]^{-3/2} < L-1.$$

For the second sum we have

$$\sum_{l=0}^{L-2}\frac{1}{(L-1-l)^3} = 1+\frac{1}{2^3}+\frac{1}{3^3}+\cdots+\frac{1}{(L-1)^3} < \zeta(3) \approx 1.202.$$

Finally, assuming $K=1$ we obtain

$$\sqrt{P_{\text{int}}} > 0.51(L-1)\chi^3. \quad (28)$$

This is the error introduced by only one pulse. The errors generated by different pulses of the protocol can accumulate.

From Eq. (28) one can see that a small parameter which characterizes the dipole-dipole interaction between the chains is $L\chi^3$ rather than χ^3. The influence of neighboring chains on each other can be minimized by introducing the corrections to the frequency [the third term in the right-hand side of Eq. (25)] and to the Rabi frequency [the second term in the right-hand side of Eq. (26)]. These corrections minimize the errors only for intermediate chains and do not minimize the error for the edge chains with $r=0$ and $r=R-1$. One can use our corrections if the number of chains R is large, so that one can neglect the edge chains, or when the chains are placed relatively close to each other, when these corrections are relatively large.

If one minimizes the errors caused by the nearest-neighboring chains, the error in the probability amplitude caused by the influence of the next-nearest neighboring chains is of the order of $\sqrt{P_{\text{int}}}/8$. Using our approach one can minimize the errors caused by the next-nearest neighboring chains and disregard the chains with $r=0,1,R-2,R-1$. This makes the error caused by the next-next-nearest neighboring chains to be of the order of $\sqrt{P_{\text{int}}}/27$ and so on.

D. Qubit displacements

One of the most serious problems that prevents building a solid-state quantum computer is manufacturing the spin system such as that shown in Fig. 1. Atoms with nonzero spin, such as ^{31}P, can be placed on the surface of a magnetically neutral substance, such as ^{28}Si, using, for example, scanning tunneling microscopy technique [34,35]. The placement of the qubits can be not perfect, so that these qubits form distorted spin chains. If one deals with a single chain, one can measure the locations of the qubits and choose the suitable pulse parameters to compensate the deviations of the qubits from their prescribed positions. On the other hand, if one implements a quantum algorithm on an ensemble of spin chains, the deviation in the location of a qubit from the perfect position (called below displacement) in a chain makes this chain different from other chains, and this error cannot be completely compensated by a proper choice of the parameters of the pulses. Here we will investigate this kind of error.

Since a qubit in a solid state is usually incorporated into the crystal lattice, the minimum possible qubit displacement is equal to the lattice constant. If the displacement happens in the direction of the magnetic field gradient (along the x axis in Figs. 1 and 6), then even a small displacement causes a relatively large change in the Larmor frequency of this qubit because the magnetic field gradient is supposed to be large. Consequently, we believe that this kind of error causes the most profound destructive effect on quantum computation in our system. Since the frequency of the displaced kth qubit considerably differs from the frequency of the pulse, this qubit will not flip and the other $(k+1)$th, $(k+2)$th, …, $(L-1)$th qubits will not flip also. For example, if $k=3$ and $L=6$ the excited state evolves as

$$|0_5 0_4 \mathbf{0}_3 0_2 \underline{0}_1 1_0\rangle \rightarrow |00\mathbf{0}\underline{0}11\rangle \rightarrow |000\underline{\mathbf{0}}111\rangle \rightarrow |0\underline{0}\mathbf{0}111\rangle \rightarrow |\underline{0}00111\rangle \rightarrow |000111\rangle,$$

where the qubit to be flipped by the corresponding pulse is underlined. One can see that the z component M of the magnetization due to the error caused by displacement of qubits is positive.

We now calculate the error due to the qubit displacement(s). It is convenient to define the dimensionless displacement v_k of the kth qubit as

$$v_k = \frac{|d\omega_k|}{\delta\omega} = \pm\frac{|dx_k|}{a}, \tag{29}$$

where dx_k is the dimensional displacement, $d\omega_k$ is the change of the Larmor frequency of the kth qubit caused by this displacement, the sign "+" must be used if one considers nuclear spins and the sign "−" must be used for electron spins. For example, the value $v_k=1/15$ corresponds to the displacement by one lattice site if the number of atoms between neighboring qubits is equal to 14 and by two lattice sites if the number of atoms between neighboring qubits is equal to 29.

If the probability $\mathcal{P}$ of a displacement is relatively large, $\mathcal{P}\geqslant 1/L$ then the number of "perfect" spin chains, where all spins are not displaced, is relatively small, so that it is important first to study the errors P_d and the magnetization M_d caused by the qubit displacements in a single spin chain.

The displaced kth qubit affects all other qubits in the chain. The transition frequency and detuning of the jth qubit $(j\neq k)$ change by the value [see Eq. (13)]

$$|\Delta_{jk}| = \frac{|J|}{2A^3}\left|\frac{1}{|k\pm v_k - j|^3} - \frac{1}{|k-j|^3}\right| \approx \frac{3|J|}{2A^3}\frac{|v_k|}{|k-j|^4} \ll \Omega_j. \tag{30}$$

It is convenient to characterize the influence of the displaced qubit on all other qubits by a small dimensionless parameter

$$\beta_{jk} = \frac{3v_k\sqrt{4K^2-1}}{2(j-k)^4}\left[\sum_{l=0}^{j-1}\frac{1}{(j-l)^3}\right]^{-1} \approx \frac{|\Delta_{jk}|}{\Omega_j} \ll 1. \tag{31}$$

Then in Eq. (10) we have

$$\sin\left(\frac{\lambda_j\tau}{2}\right) \approx 1 - \frac{\pi^2}{32}\beta_{jk}^4 \approx 1, \quad \cos\left(\frac{\lambda_j\tau}{2}\right) \approx -\frac{\pi}{2}\beta_{jk}^2.$$

When the jth qubit is flipped in the excited state we have $\Delta=\Delta_{jk}$ instead of $\Delta=0$ and the error is

$$P_{jk} \approx \frac{\Delta_{jk}^2}{\lambda_{jk}^2} = \frac{1}{2}\beta_{jk}^2 \approx \frac{9(4K^2-1)}{8(j-k)^8\zeta^2(3)}v_k^2.$$

For example, for $v_k=1/20$ and $K=1$ we have

$$P_{k\pm1,k} \approx 0.006, \quad P_{k\pm2,k} \approx 2.3\times 10^{-5}.$$

The probability of the transition from the ground state caused by the deviation in the detuning is

$$P'_{jk} \approx \frac{\pi^2(4K^2-1)}{128K^4}\beta_{jk}^2.$$

For $K=1$ the error caused by the ground state $P'_{jk}\approx 0.25\beta_{jk}^2$ is of the same order as the error P_{jk} caused by the excited state. Below we will neglect the errors P_{jk} and P'_{jk} caused by the influence of the displaced qubit on all other qubits as being small compared to the other errors.

We now estimate the probability P_{kk} caused by the kth pulse on the kth displaced qubit. Since $\alpha\sim 1/|\delta\omega|$ it is convenient to measure the dimensionless frequency displacement in units of $1/\alpha$, so that the change in the transition frequency of the kth qubit caused by its displacement is proportional to v_k/α. We first analyze the action of the kth pulse on the excited state. Instead of the resonant transition with the detuning $\Delta_k=0$ we have the transition with the detuning $\Delta_k=\pm v_k\delta\omega$, where the sign "+" corresponds to the displacement in the positive x direction and the sign "−" corresponds to the displacement in the opposite direction.

If $k\neq 0$ then the amplitude of the excited state is

$$|C_{q'}| = \frac{1}{\sqrt{2}}\frac{1}{\sqrt{1+(v_k/\alpha_k)^2}}\sin\left[\frac{\pi}{2}\sqrt{1+\left(\frac{v_k}{\alpha_k}\right)^2}\right],$$

where

$$\alpha_k = \frac{\Omega_k}{|\delta\omega|} = \alpha\sum_{l=0}^{k-1}\frac{1}{|k-l|^3}. \tag{32}$$

The error generated by the excited state is

$$P_{kk} \equiv P_d = \frac{1}{2}\left\{1 - \frac{1}{1+(v_k/\alpha_k)^2}\sin^2\left[\frac{\pi}{2}\sqrt{1+\left(\frac{v_k}{\alpha_k}\right)^2}\right]\right\}. \tag{33}$$

One can see that the ratio v_k/α characterizes the error caused by the displacement v_k: if $v_k/\alpha\to 0$ then $P_d\to 0$, otherwise $P_d\to 1/2$.

The error caused by the action of the kth pulse, $k\neq 0$, on the ground state of the superposition is

$$P'_d(\pm) = \frac{1}{2\left[1+\left(\sqrt{4K^2-1}\mp\frac{v_k}{\alpha_k}\right)^2\right]} \times\sin^2\left[\frac{\pi}{2}\sqrt{1+\left(\sqrt{4K^2-1}\mp\frac{v_k}{\alpha_k}\right)^2}\right]. \tag{34}$$

For a large magnetic field gradient the error P'_d is small,

$$P'_d \sim \frac{1}{(v_k/\alpha_k)^2}, \quad \frac{|v_k|}{\alpha_k} \gg 1. \tag{35}$$

For $k=0$ the probability of the excited state after implementation of the Hadamard transform on the displaced qubit is

$$\eta = |C_1|^2 = \frac{1}{1+(v_0/\alpha_0)^2}\sin^2\left[\frac{\pi}{4}\sqrt{1+\left(\frac{v_0}{\alpha_0}\right)^2}\right], \tag{36}$$

where $\alpha_0=\Omega_H/|\delta\omega|$, Ω_H is the Rabi frequency of the pulse implementing the Hadamard transform. Here and in the sequel we take $\alpha_0=\alpha_1=\alpha$. The probability of error generated by this pulse is

$$\left|\frac{1}{2}-|C_0|^2\right| + \left|\frac{1}{2}-|C_1|^2\right|,$$

where $|C_0|^2=1-|C_1|^2$. Assuming that the other pulses of the protocol do not generate error, we obtain that the error due to the displaced zeroth qubit is

$$P_{00} \equiv P''_d = \left|\frac{1}{2}-(1-\eta)\right| + \left|\frac{1}{2}-\eta\right| = 1-2\eta. \tag{37}$$

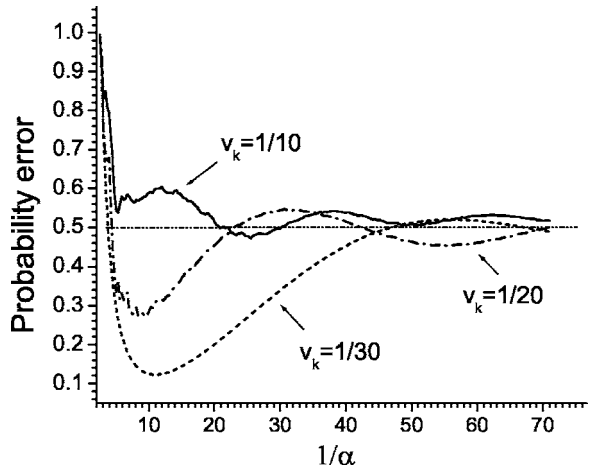

FIG. 7. The probability error P obtained using numerical solution as a function of $1/\alpha$ for different values of v_k. The displaced qubit is located at the center of the chain $L=9$.

Since $1/\alpha \sim |\delta\omega|$ decreasing $|\delta\omega|$ decreases the error P_d. On the other hand, due to Eqs. (20) and (21), the error $P_{\rm nr}$ caused by the nonselective excitations (nonresonant transitions) increases with $|\delta\omega|$ decreasing. The total probability error for $k \neq 0$ is

$$P = P_{\rm nr} + P_d + P'_d(-), \tag{38}$$

where the qubit is assumed to be displaced in the negative x direction. In Fig. 7 we plot the probability error P, defined as

$$P = \left| \frac{1}{2} - |C_0(T)|^2 \right| + \left| \frac{1}{2} - |C_{2^L-1}(T)|^2 \right|, \tag{39}$$

which was obtained using exact numerical solution for $k \neq 0$. In Eq. (39) T is the total time of implementation of the entanglement protocol. When $1/\alpha$ is small the probability error P is large due to the nonresonant excitations. When $1/\alpha$ is large P is large because the displaced qubit does not flip. From the results presented in Fig. 7 one can see that if the displacement is relatively large ($v_k=1/10$), then the error is always large and the entanglement protocol cannot be optimized for any parameters of the model.

As follows from Fig. 7, the magnitude of P becomes close to $1/2$ and relatively independent of L and $1/\alpha$ when $1/\alpha$ is large, i.e., when $(v_k/\alpha)^2 \gg 1$. For these parameters we have mostly two states in the superposition: the ground state and the partially excited state. For example, if the kth qubit is displaced, $k=3$ and $L=6$, then instead of the desired entangled state

$$\frac{1}{\sqrt{2}}(|00000\rangle + |111111\rangle) \tag{40}$$

we have the state

$$\frac{1}{\sqrt{2}}(|00000\rangle + |000111\rangle).$$

The z component of the magnetization M_d due to a displaced qubit can be estimated using the probability error. If $k \neq 0$ the probability P_d is mostly independent of the position k of the displaced qubit in the chain. Unlike P, M_d is large (and positive) if the displaced qubit is located in the beginning of the spin chain and relatively small if the displaced qubit is located in the end of the chain. For example, if k is the number of the displaced qubit and $k=1$ then the excited state is ($L=6$) $|000001\rangle$ instead of $|111111\rangle$ and the entangled state is

$$\frac{1}{\sqrt{2}}(|00000\rangle + |000001\rangle) \tag{41}$$

instead of the state (40). The z component of the magnetization for the state (41) is $M_d=(5/6)$. If the displaced qubit is located in the end of the chain, for example, if $k=6$, then the value of M for the state

$$\frac{1}{\sqrt{2}}(|00000\rangle + |011111\rangle) \tag{42}$$

is $M_d=(1/6)$.

In order to relate M with the probability error consider the two situations when $k \neq 0$ and when $k=0$. If $k \neq 0$ we note that after implementation of the entanglement protocol on the spin chain with a displaced qubit in the register there are mostly four quantum states: the ground state with the probability $1/2-P'_d(\pm)$, the error state with the probability $P'_d(\pm)$ created from the ground state, the error state with the probability P_d created from the excited state, and the fully excited state $|11\cdots11\rangle$ with the probability $1/2-P_d$. Next, we assume that the position of the displaced qubit in the chain is random. By averaging over many random realizations we obtain that the two error states do not contribute to M. For example, the z component of the magnetization of the partially excited state in Eq. (41) is $M=\frac{1}{2}\frac{4}{6}$ while in Eq. (42) $M=-\frac{1}{2}\frac{4}{6}$, so that the average of these two contributions is zero. The contribution to the M due to the fully excited state is $-\left(\frac{1}{2}-P_d\right)$. By adding all these contributions we obtain

$$M_d = \frac{1}{2} - P'_d(\pm) - \left(\frac{1}{2} - P_d\right) = P_d - P'_d(\pm). \tag{43}$$

If $k=0$ there are mostly two states in the register: the ground state with the probability $1-\eta$ and the fully excited state with the probability η, where η is given by Eq. (36). The magnetization due to the displaced zeroth qubit is

$$M''_d = 1 - 2\eta = P''_d. \tag{44}$$

The total magnetization is

$$M = M_{\rm nr} + M_d, \quad \text{for } k \neq 0,$$

$$M = M_{\rm nr} + M''_d, \quad \text{for } k = 0, \tag{45}$$

where $M_{\rm nr}$ is given by Eqs. (22) and (23).

Assume that we have an ensemble of R spin chains and the probability of a qubit to be displaced by one lattice site is ξ. If, for example, $\xi=1/L$, then on average one qubit in each chain is displaced, if $\xi=1/(nL)$ then on average one qubit in

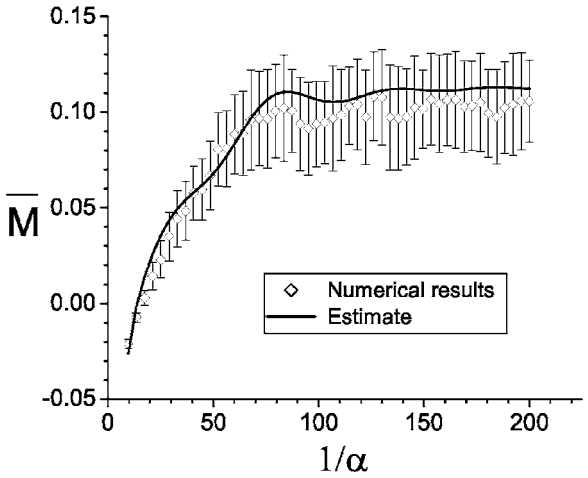

FIG. 8. The z component of the magnetization $\bar{M}$ as a function of $1/\alpha$ for $R=100$ spin chains with $L=7$ qubits in each chain. The numerical results are averaged over 50 realizations of different 7×100 qubit ensembles with randomly chosen displaced qubits, $\xi=1/(5L)$. The displacements are in the random directions along the x axis. The estimate is calculated using Eq. (47). $v_k=1/20$, $K=1$.

n chains is displaced. The total number of displaced qubits with $k\neq0$ is on average $\xi R(L-1)$ and the total number of displaced qubits with $k=0$ is on average ξR, so that

$$\bar{M}_d=\frac{\xi}{L}\left[\sum_{k=1}^{L-1}(P_{d,k}-P'_{d,k})+P''_d\right],$$

$$P'_{d,k}\equiv\frac{1}{2}[P'_{d,k}(-)+P'_{d,k}(+)], \tag{46}$$

where $P_{d,k}$ and $P'_{d,k}$ depend on k through the dependence of α_k on k in Eq. (32). We calculated numerically

$$\bar{M}=M_{\rm nr}+\bar{M}_d \tag{47}$$

as a quantum-mechanical average for 100 noninteracting spin chains with randomly chosen displaced qubits and random displacement directions (in positive and negative directions along the x axis). In Fig. 8 we plot $\bar{M}$ as a function of α obtained using the exact numerical solution and our estimate given by Eq. (47) for $\xi=1/(5L)$. As follows from the figure our estimate (47) is a good analytical approximation of M. In particular, Eq. (47) can be used for estimation of M when the number of qubits L in each chain is large.

E. Fluctuations of permanent magnetic field

The error $P_{\rm osc}$ caused by fluctuations of permanent magnetic field $d\omega$ due, for example, to unwanted oscillations of the dc current in wires needed for creating the magnetic field gradient can be estimated using Eqs. (33) and (34). Instead of the dimensionless deviation v_k we introduce the average dimensionless deviation $\bar{v}$ as

$$\bar{v}=\left|\frac{\overline{d\omega}}{\delta\omega}\right|,$$

where $|\overline{d\omega}|$ is the average deviation of the transition frequency of a qubit from the optimal value caused by a fluctuation of the current in the wires creating the magnetic field gradient. We assume that this deviation is small, $(\bar{v}/\alpha)^2\ll1$.

The average error due to unwanted transitions from the excited and ground states for $k\neq0$ is [see Eqs. (33) and (34)]

$$P_{\rm osc}(k)=P'_{\rm osc}(k)+P''_{\rm osc}(k), \tag{48}$$

where

$$P'_{\rm osc}(k)=\frac{\pi^2(4K^2-1)}{128K^4}\left(\frac{\bar{v}}{\alpha_k}\right)^2,\quad P''_{\rm osc}(k)=\frac{1}{2}\left(\frac{\bar{v}}{\alpha_k}\right)^2.$$

Here $P'_{\rm osc}(k)$ and $P''_{\rm osc}(k)$ are the probability errors created from, respectively, the ground and excited states by action of the kth pulse of the protocol. For $k=0$ (Hadamard gate) from Eq. (36) the probability of the excited state is

$$\eta\approx\frac{1}{2}\left[1+\left(\frac{\pi}{4}-1\right)\left(\frac{\bar{v}}{\alpha_0}\right)^2\right],$$

so that the average error is

$$P_{\rm osc}(k=0)=1-2\eta=\left(1-\frac{\pi}{4}\right)\left(\frac{\bar{v}}{\alpha_0}\right)^2.$$

The average total error due to the nonresonant transitions and oscillations of the magnetic field is

$$P=P_{\rm nr}+P_{\rm osc}(0)+\sum_{k=1}^{L-1}P_{\rm osc}(k). \tag{49}$$

Since $P_{\rm nr}\sim\alpha^2$ and $P_{\rm osc}(k)\sim1/\alpha^2$ there is an optimal value of α

$$\alpha_{\rm opt}\approx\left[\frac{\bar{v}^2}{(-0.82+0.86L)}\right]^{1/4}\times\left\{1-\frac{\pi}{4}+\left[\frac{1}{2}+\frac{\pi^2(4K^2-1)}{128K^4}\right]\left[\frac{L-1}{\zeta^2(3)}+0.6\right]\right\}^{1/4}, \tag{50}$$

where P is minimal. For example, for $\bar{v}=10^{-4}$, $L=9$, and $K=1$ we have $\alpha_{\rm opt}\approx9.08\times10^{-3}$.

In Fig. 9 we plot the error P caused by action of both nonresonant transitions and unwanted oscillations of the permanent magnetic field. Numerical results are obtained by diagonalization of the full Hamiltonian matrix in the rotating frame. The random values of v for the numerical results have the Gaussian distribution with the zero average and dispersion equal to $\bar{v}$. In our model a magnetic field fluctuation is constant (and random) during each pulse. Each point of the numerical results is the average over 30 realizations with the random values of v. One can see from the figure that for $\alpha<\alpha_{\rm opt}$ the error is mostly defined by the fluctuations of the permanent magnetic field and P decreases with increasing α as $P\sim1/\alpha^2$. For $\alpha>\alpha_{\rm opt}$ the error is due to the nonresonant excitations and $P\sim\alpha^2$. From Fig. 9 one can see that our

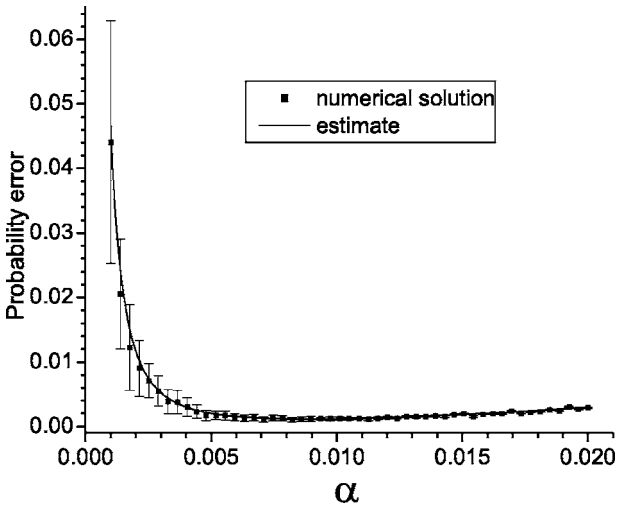

FIG. 9. The error caused by nonresonant transitions and unwanted oscillations of the permanent magnetic field as a function of α for $\bar{v}=10^{-4}$ and $L=9$. The estimate is obtained using Eq. (49).

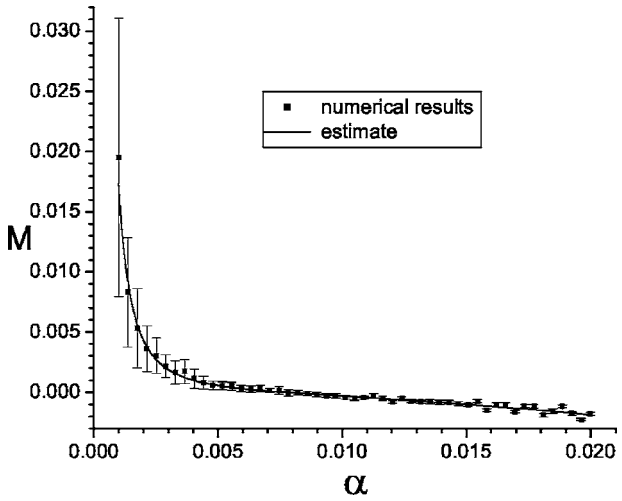

FIG. 10. M as a function of α in the presence of unwanted oscillations of the external permanent magnetic field. The parameters are the same as in Fig. 9. The estimate is calculated using Eq. (52).

estimate (49) correctly describes the probability error in the presence of unwanted oscillations of the permanent magnetic field.

Now we will calculate the z component of the magnetization $M_{\rm osc}$. Consider a typical example with $L=4$ qubits. If the first pulse of the protocol ($k=1$) generates error and other pulses do not generate the error, then after implementation of the entanglement algorithm there are four states in the register with the following probabilities:

$$|0000\rangle, \quad \frac{1}{2} - P'_{\rm osc}(1),$$

$$|1110\rangle, \quad P'_{\rm osc}(1),$$

$$|1111\rangle, \quad \frac{1}{2} - P''_{\rm osc}(1),$$

$$|0001\rangle, \quad P''_{\rm osc}(1).$$

The value of $M_{\rm osc}$ for this superposition is

$$P''_{\rm osc}(1) - P'_{\rm osc}(1) + \frac{L-2}{L}[P''_{\rm osc}(1) - P'_{\rm osc}(1)].$$

If all the pulses of the protocol generate the error, then the z component of the magnetization is

$$M_{\rm osc} = P_{\rm osc}(0) + \sum_{k=1}^{L-1}\left[1 + \frac{L-2k}{L}\right][P''_{\rm osc}(k) - P'_{\rm osc}(k)]. \tag{51}$$

In Fig. 10 we compare our estimate

$$M = M_{\rm nr} + M_{\rm osc} \tag{52}$$

with the results of numerical simulations for the same values of α as in Fig. 9. One can see that our estimate gives us a good approximation of M.

VI. DISCUSSION

We considered the implementation of entanglement in a two-dimensional ensemble of spin chains. We demonstrated that the entanglement can be created in the system with a long-range interaction, such as dipole-dipole interaction, and the error caused by this interaction can be significantly reduced by optimization of parameters of the pulses.

If the entanglement is implemented with no error, then $M=0$. We considered different mechanisms which can generate errors and make $M\neq 0$. By experimental measurement of M for different parameters one can define the most important mechanism responsible for the errors and optimize the design using the obtained information. The output signal can be enhanced by the multiple copies of the spin states. The most important dimensionless parameter characterizing the model is α which is proportional to the ratio of the Rabi frequency to the difference $\delta\omega$ between the Larmor frequencies of neighboring qubits. We now summarize the influence of different kinds of errors on M.

(1) *Decoherence*. Decreasing α by decreasing the Rabi frequency one can increase the total time of implementation of the algorithm and increase $|M|$. The value of M is positive. Decreasing α by increasing the gradient $|\delta\omega|$ does not influence M.

(2) *Nonselective excitations (nonresonant transitions)*. Decreasing α by decreasing the Rabi frequency or increasing $|\delta\omega|$ one can decrease $|M|$. The value of M is negative.

(3) Influence of different chains on each other can be estimated in the following way. (a) One implements the protocol using the frequency ν and the Rabi frequency Ω given by Eqs. (13)–(15). (b) One takes into consideration the influence of neighboring chains on each other and modifies the frequencies and the Rabi frequencies using Eqs. (25) and (26). If $|M|$ decreases then the error is mostly caused by the dipole-dipole interactions between the spins of different chains.

(4) The error is caused by displacements of the qubits if one observes the following properties: (a) if the gradient $\delta\omega$

is relatively large [$(v_k/\alpha)^2 \gg 1$ in Eq. (33)] M is positive and independent of α; (b) the same effect is observed if the distance a between the qubits is relatively small and the relative displacement of the kth qubit $|v_k| = |dx_k|/a$, where dx_k is the displacement of the kth qubit along the chain, is relatively large, $|v_k| \geqslant 1/10$; (c) if the gradient $\delta\omega$ is relatively small ($|v_k|/\alpha \geqslant 1$) increasing α we decrease $|M|$ and $M > 0$. The latter effect is opposite to the influence of α in nonresonant excitations where increasing α we increase $|M|$ and $M < 0$.

(5) *Unwanted fluctuations of permanent magnetic field.* When α increases M decreases, $M > 0$, and $M \sim 1/\alpha^2$.

We did not consider all possible mechanisms such as, for example, the influence of magnetic impurities in the substrate [36]. Some processes not considered here in detail, such as the decoherence caused by environment, can be investigated by using the density matrix if one finds that this kind of decoherence is the most important mechanism responsible for the errors.

In conclusion, we note that the presence of noise in the measurement of $\mathcal{M}_z$ is a limiting factor. This noise in an experimental setup could make it hard to measure small changes in $\mathcal{M}_z$ and our technique can be useful for systems with relatively large errors. The sensitivity in our system can be increased by increasing the number of spins. For example, a superconducting quantum interference device (SQUID) can be used for measurement of magnetization from as small as 40 qubits [37] by measuring the magnetic flux through the loop. The SQUID loop size (of the order of 3 μm $\times$ 3 μm) makes it possible to allocate thousands of qubits inside the loop. Increasing the number of qubits to, for example, 4000 would allow one to measure relatively small variations in $\mathcal{M}_z$ and to test our theoretical results.

ACKNOWLEDGMENTS

This work was carried out under the auspices of the National Nuclear Security Administration of the U.S. Department of Energy at Los Alamos National Laboratory under Contract No. DE-AC52–06NA25396.

[1] P. W. Shor, in *Proceedings of the 35th Annual Symposium on the Foundations of Computer Science*, edited by S. Goldwasser (IEEE Computer Society, Los Alamitos, 1994), p. 124.
[2] G. P. Berman, G. D. Doolen, R. Mainieri, and V. I. Tsifrinovich, *Introduction to Quantum Computers* (World Scientific, Singapore, 1998).
[3] D. P. DiVincenzo, in *Mesoscopic Electron Transport*, edited by L. Kowenhoven, G. Sohn, and L. Sohn, Vol. 345 of NATO Advanced Studies Institute Series E: Applied Sciences (Kluwer Academic, Dordrecht, 1997).
[4] M. Mehring, J. Mende, and W. Scherer, Phys. Rev. Lett. **90**, 153001 (2003).
[5] M. Mehring, W. Scherer, and A. Weidinger, Phys. Rev. Lett. **93**, 206603 (2004).
[6] M. Howard, J. Twamley, C. Wittmann, T. Gaebel, F. Jelezko, and J. Wrachtrup, quant-ph/0601167 (unpublished).
[7] J. Baugh, O. Moussa, C. A. Ryan, A. Nayak, and R. Laflamme, Nature (London) **438**, 470 (2005).
[8] J. Baugh, O. Moussa, C. A. Ryan, R. Laflamme, C. Ramanathan, T. F. Havel, and D. G. Cory, quant-ph/0510115 (unpublished).
[9] I. Chiorescu, Y. Nakamura, C. J. P. M. Harmans, and J. E. Mooij, Science **299**, 1869 (2003).
[10] Yu. A. Pashkin, T. Yamamoto, O. Astafiev, Y. Nakamura, D. V. Averin, and J. S. Tsai, Nature (London) **421**, 823 (2003).
[11] O. Astafiev, Yu. A. Pashkin, T. Yamamoto, Y. Nakamura, and J. S. Tsai, Phys. Rev. B **69**, 180507(R) (2004).
[12] B. E. Kane, Nature (London) **393**, 133 (1998).
[13] T. D. Ladd, J. R. Goldman, F. Yamaguchi, and Y. Yamamoto, E. Abe, and K. M. Itoh, Phys. Rev. Lett. **89**, 017901 (2002).
[14] V. N. Smelyanskiy, A. G. Petukhov, and V. V. Osipov, Phys. Rev. B **72**, 081304(R) (2005).
[15] W. Harneit, Phys. Rev. A **65**, 032322 (2002).
[16] T. Almeida Murphy, Th. Pawlik, A. Weidinger, M. Höhne, R. Alcala, and J.-M. Spaeth, Phys. Rev. Lett. **77**, 1075 (1996).
[17] A. Weidinger, M. Waiblinger, B. Pietzak, and T. Almeida Murphy, Appl. Phys. A: Mater. Sci. Process. **66**, 287 (1998).
[18] J. Twamley, Phys. Rev. A **67**, 052318 (2003).
[19] G. P. Berman, V. I. Tsifrinovich, and D. L. Allara, Phys. Rev. B **66**, 193406 (2002).
[20] A. Tamulis, V. I. Tsifrinovich, S. Tretiak, G. P. Berman, and D. L. Allara, quant-ph/0307136 (unpublished).
[21] Z. Rinkevicius, G. P. Berman, D. L. Allara, V. I. Tsifrinovich, and S. Tretiak, quant-ph/0411202 (unpublished).
[22] G. P. Berman, D. I. Kamenev, R. B. Kassman, and V. I. Tsifrinovich, Int. J. Quantum Inf. **1**, 51 (2003).
[23] G. P. Berman, G. D. Doolen, G. V. Lòpez, and V. I. Tsifrinovich, Phys. Rev. A **61**, 062305 (2000).
[24] G. P. Berman, G. D. Doolen, D. I. Kamenev, and V. I. Tsifrinovich, Phys. Rev. A **65**, 012321 (2002).
[25] G. P. Berman, D. I. Kamenev, and V. I. Tsifrinovich, J. Appl. Math. **2003**, 35 (2003).
[26] G. P. Berman, D. I. Kamenev, and V. I. Tsifrinovich, *Perturbation Theory for Solid-State Quantum Computation with Many Quantum Bits* (Rinton Press, Princeton, 2005).
[27] G. P. Berman, D. K. Campbell, and V. I. Tsifrinovich, Phys. Rev. B **55**, 5929 (1997).
[28] D. I. Kamenev, G. P. Berman, R. B. Kassman, and V. I. Tsifrinovich, Int. J. Quantum Inf. **2**, 323 (2004).
[29] S. Knorr, A. Grupp, M. Mehring, M. Wailblinger, and A. Weidinger, in *Electronic Properties of Novel Materials and Molecular Nanostructures: XIV International Winterschool/Euroconference*, edited by H. Kuzmany, J. Fink, M. Mehring, and S. Roth, AIP Conf. Proc. No. 544 (AIP, Melville, 2000), p. 191.
[30] M. Drndić, K. S. Johnson, J. H. Thywissen, M. Prentis, and R. M. Westervelt, Appl. Phys. Lett. **72**, 2906 (1998).
[31] J. R. Goldman, T. D. Ladd, F. Yamaguchi, and Y. Yamamoto, Appl. Phys. A: Mater. Sci. Process. **71**, 11 (2000).
[32] D. Suter and K. Lim, Phys. Rev. A **65**, 052309 (2002).

[33] D. A. Lidar and J. H. Thywissen, J. Appl. Phys. **96**, 754 (2004).
[34] J. L. O'Brien, S. R. Schofield, M. Y. Simmons, R. G. Clark, A. S. Dzurak, N. J. Curson, B. E. Kane, N. S. McAlpine, M. E. Hawley, and G. W. Brown, Phys. Rev. B **64**, 161401(R) (2001).
[35] J. R. Tucker and T.-C. Shen, Solid-State Electron. **42**, 1061 (1998).
[36] G. P. Berman, B. M. Chernobrod, V. N. Gorshkov, and V. I. Tsifrinovich, Phys. Rev. B **71**, 184409 (2005).
[37] C. I. Pakes, P. W. Josephs-Franks, R. P. Reed, S. G. Corner, and M. S. Colclough, IEEE Trans. Instrum. Meas. **50**, 310 (2001).